Supporting Information

Construction of Hierarchical Carbon Coated Fe_3O_4 Nanorods Anode for 2.6 V Aqueous Asymmetric Supercapacitors with Ultrahigh Energy Density

Zhongyou Peng[a,b], Jun Huang[a,b], Ying Wang[a,b], Kai Yuan[a,b], Licheng Tan[a,b], Yiwang Chen*[a,b,c]*

[a] College of Chemistry, Nanchang University, 999 Xuefu Avenue, Nanchang 330031, China

[b] Institute of Polymers and Energy Chemistry (IPEC), Nanchang University, 999 Xuefu Avenue, Nanchang 330031, China.

[c] Institute of Advanced Scientific Research (iASR), Jiangxi Normal University, 99 Ziyang Avenue, Nanchang 330022, China.

*Corresponding Authors: tanlicheng@ncu.edu.cn (L. Tan); ywchen@ncu.edu.cn (Y. Chen).

Author contributions: Z. P. and J. H. contributed equally to this work.

***Calculations*:**

To construct the highly efficient asymmetric supercapacitors, the mass loading of the cathode (CC/CW/MnO_2) and anode (CC/CW/Fe_3O_4@C) was balanced according to the following equation:

$$\frac{m_+}{m_-} = \frac{C_{s-} \Delta V_-}{C_{s+} \Delta V_+} \quad (1)$$

where *m* (g) is the mass, *Cs* (F g^{-1}) is the specific capacitance, and ΔV (V) is the voltage range for cathode and anode, respectively.

The specific capacitance *C* (F g^{-1}) was calculated using the following formula:

$$C = \frac{I}{m dV/dt} \quad (2)$$

where *I* (A) is the discharge current, *m* (g) is the mass of the active material, and the value of *dV*(V)/*dt* (s) represents the slope of the discharge curve in the GCD measurement.

Based on the total mass of the active materials of the anode and cathode, the energy density (*E*) and power density (*P*) were calculated using the following equations, respectively:

$$E = \frac{C\,(\Delta V)^2}{2 \times 3.6} \quad (3)$$

$$P = \frac{E \times 3600}{\Delta t} \quad (4)$$

where *C* (F g^{-1}) is the specific capacitance, ΔV (V) is the potential window, and Δt (s) is the discharge time. The units of energy density *E* (Wh kg^{-1}) and power density *P* (W kg^{-1}), respectively.

The areal capacitance C_A (mF cm^{-2}) and volumetric capacitance C_V (mF cm^{-3}) were calculated from the GCD curves based on equation (5):

$$C_A = \frac{I\Delta t}{S\Delta V} \; or \; C_V = \frac{I\Delta t}{SD\Delta V} \tag{5}$$

The areal energy density E_A (mWh cm^{-2}), volumetric energy density E_V (mWh cm^{-3}), areal power density P_A (mW cm^{-2}) and volumetric power density P_v (mW cm^{-3}) were defined according to equations (6) and (7), respectively:

$$E_A = \frac{C_A \Delta V^2}{7200} \; or \; E_V = \frac{C_V \Delta V^2}{7200} \tag{6}$$

$$P_A = \frac{E_A \times 3600}{\Delta t} \; or \; P_V = \frac{E_V \times 3600}{\Delta t} \tag{7}$$

where I (mA) is the discharge current, Δt (s) is the discharge time, ΔV (V) is the potential window, S (cm^{-2}) is the geometric surface of the active material on carbon cloth, and D (cm) is the thickness of the ASCs (The area and thickness of CC/CW/MnO_2//CC/CW/Fe_3O_4@C ASC device is about 1 cm^2 and 0.08 cm. Hence, the whole volume of our ASC device is about 0.08 cm^3).

The contribution from diffusion-controlled process and surface reaction of anode and cathode can be evaluated by using CV curves.[1,2] The relationship between current (I) and scan rate (v) can be written as:

$$I = {}_a b^v \tag{8}$$

Where a and b are constant can be obtained from log v versus log I plots. When b= 0.5 indicates an ideal diffusion-dominated process and when b = 1.0 indicates surface-determined capacitive-controlled behavior. Furthermore, the capacitive contribution to the total current can be differentiated quantitively by using the following equations:

$$I(V) = k_1 v + k_2 v^{\frac{1}{2}} \tag{9}$$

$$\frac{I(V)}{v^{\frac{1}{2}}} = k_1 v^{\frac{1}{2}} + k_2 \tag{10}$$

Where I is the current density at a voltage (V), v is the scan rate (mV s^{-1}), k_1 and k_2 can be obtained from the slope and intercept, respectively. Where k_1v can be attributed to the current from surface capacitance contribution, while $k_2v^{1/2}$ is indexed to the diffusion process.

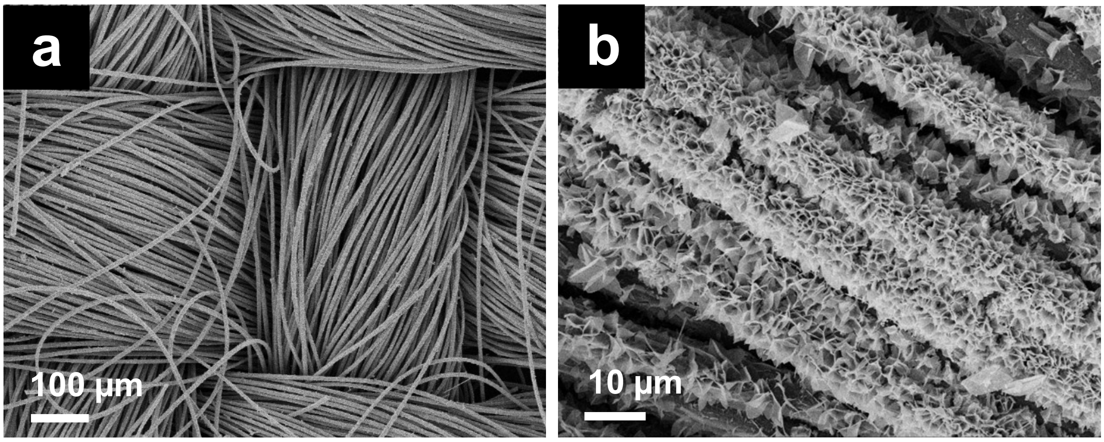

Figure S1. SEM images of CC/CW.

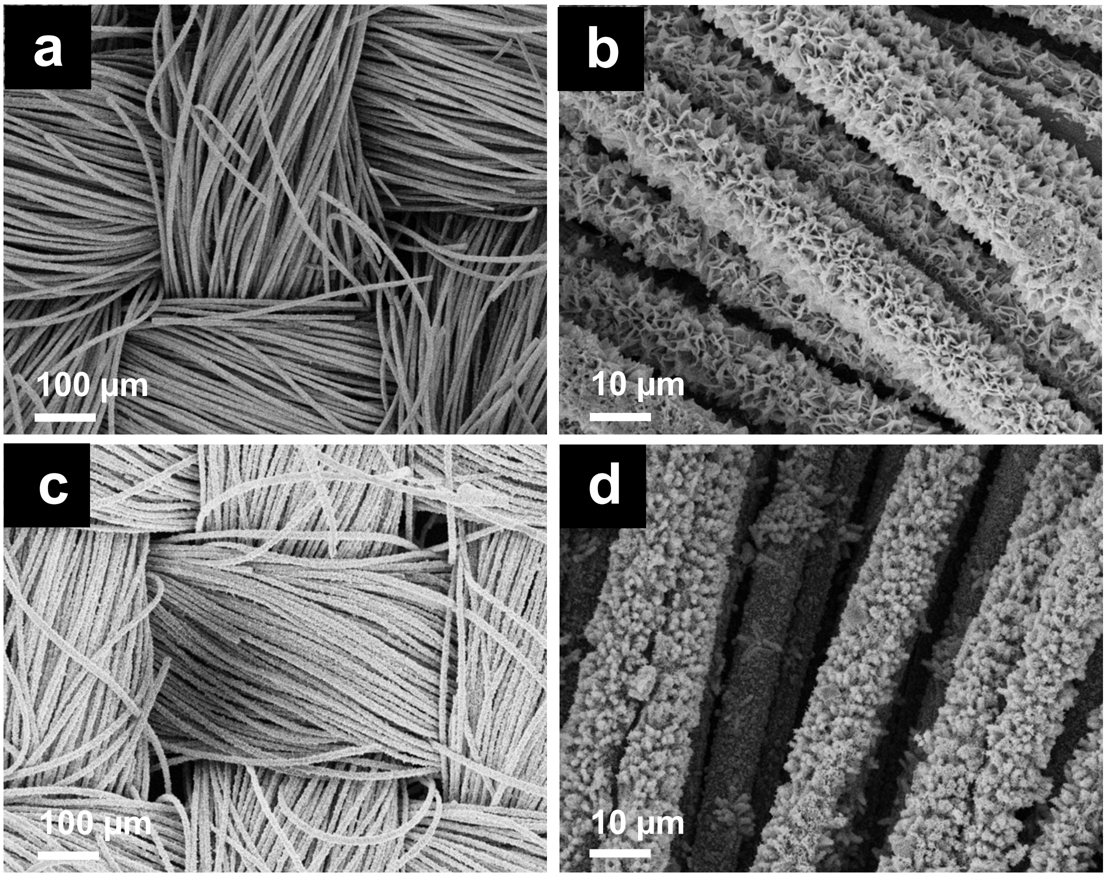

Figure S2. SEM images of (a,b) $CC/CW/Fe_3O_4$ and (c,d) $CC/CW/Fe_3O_4@C$.

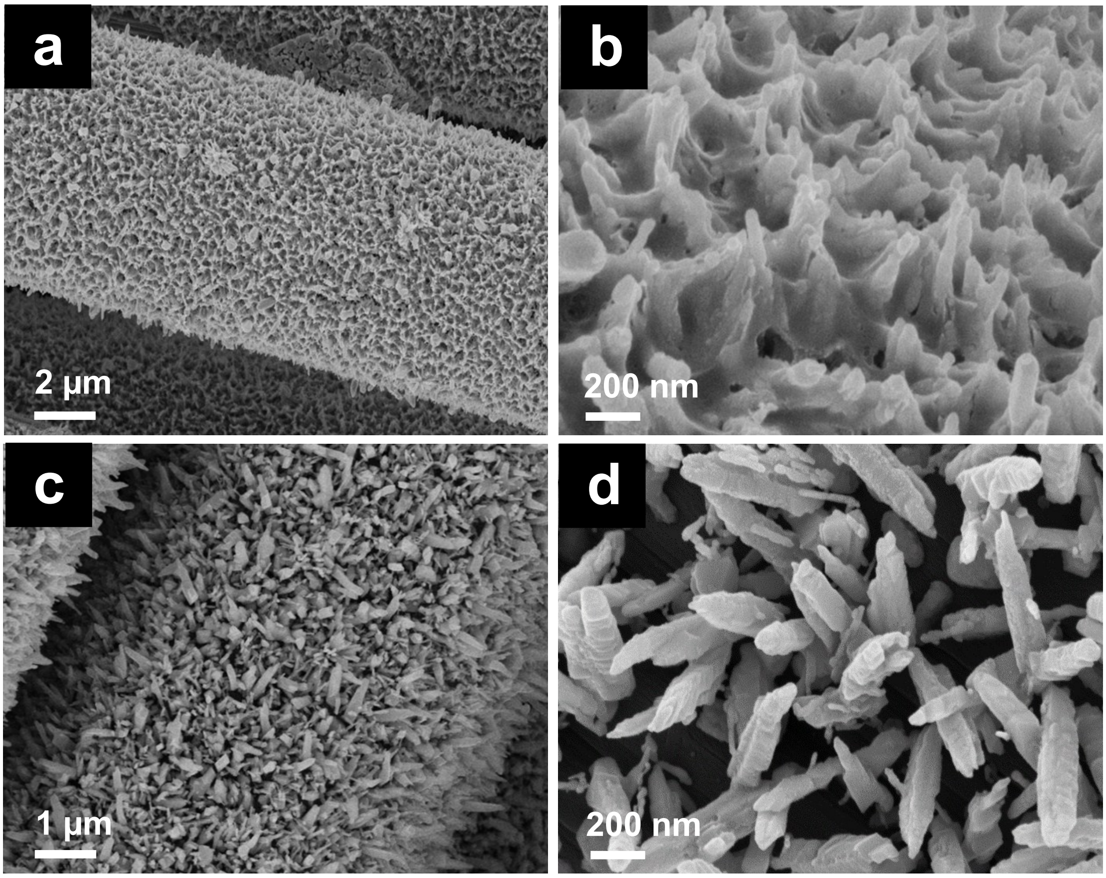

Figure S3. SEM images of (a,b) $CC/Fe_3O_4@C$ and (c,d) CC/Fe_3O_4.

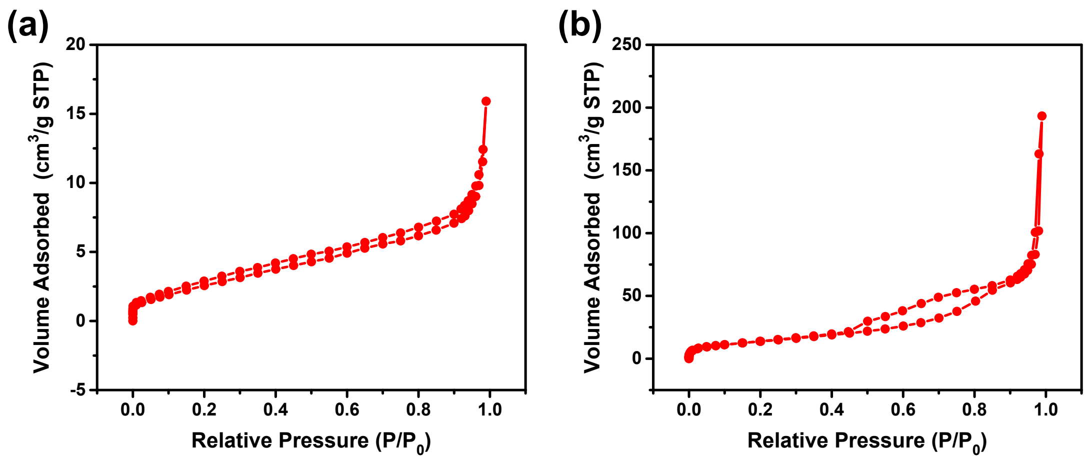

Figure S4. Nitrogen adsorption-desorption isotherms for (a) FeOOH NRAs and (b) Fe_3O_4 NRAs.

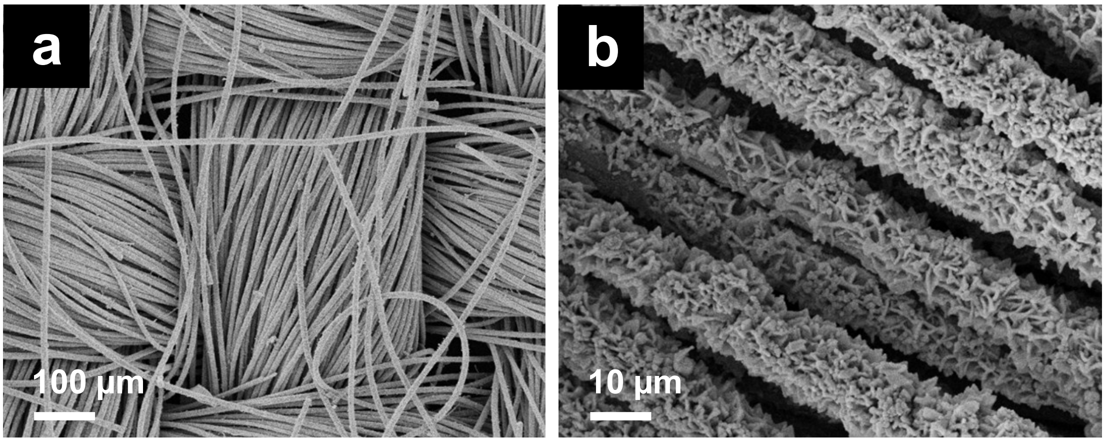

Figure S5. SEM images of CC/CW/MnO_2.

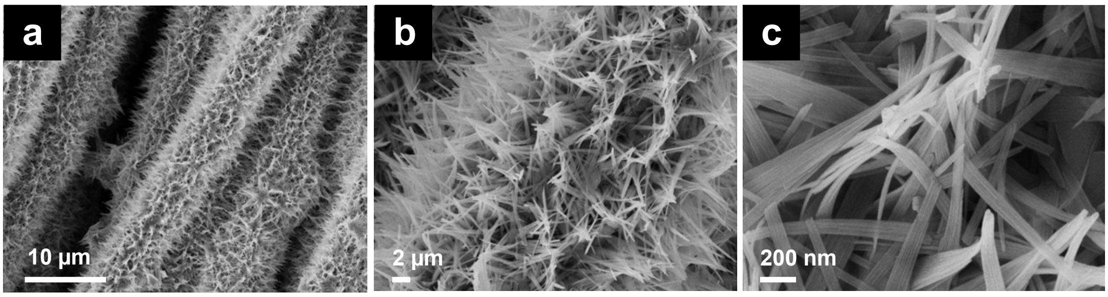

Figure S6. SEM images of CC/MnO_2.

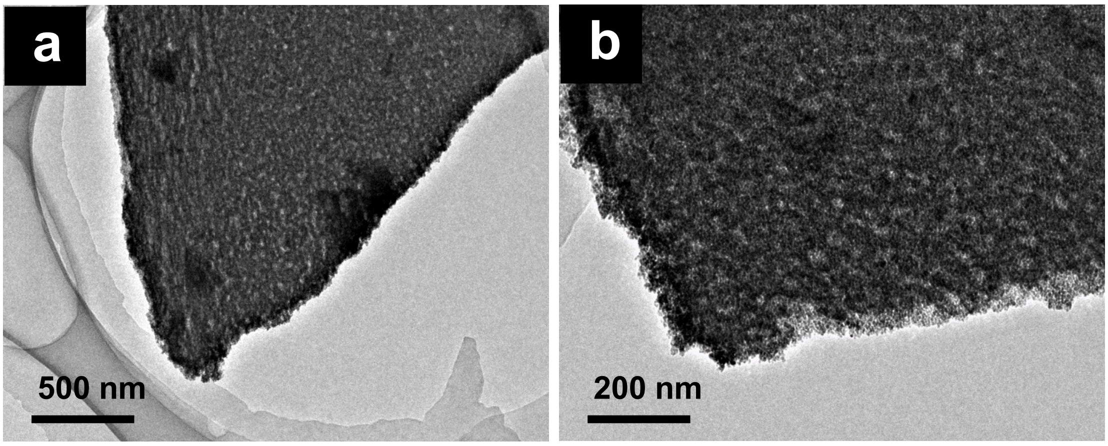

Figure S7. TEM images of CW.

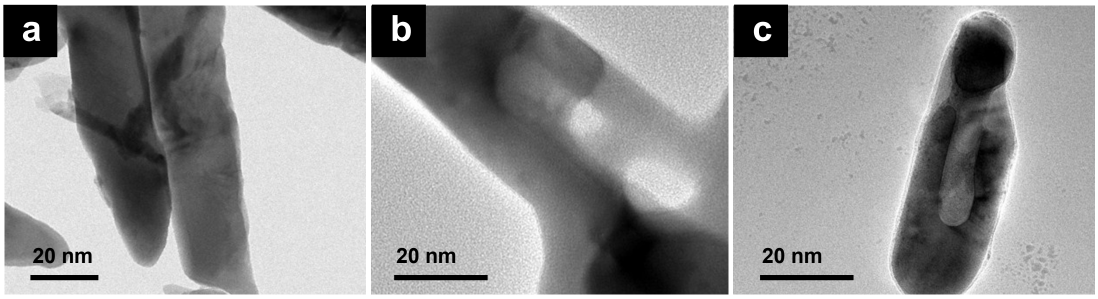

Figure S8. TEM images of (a) FeOOH NRAs, (b) Fe_3O_4 NRAs and (c) Fe_3O_4@C NRAs.

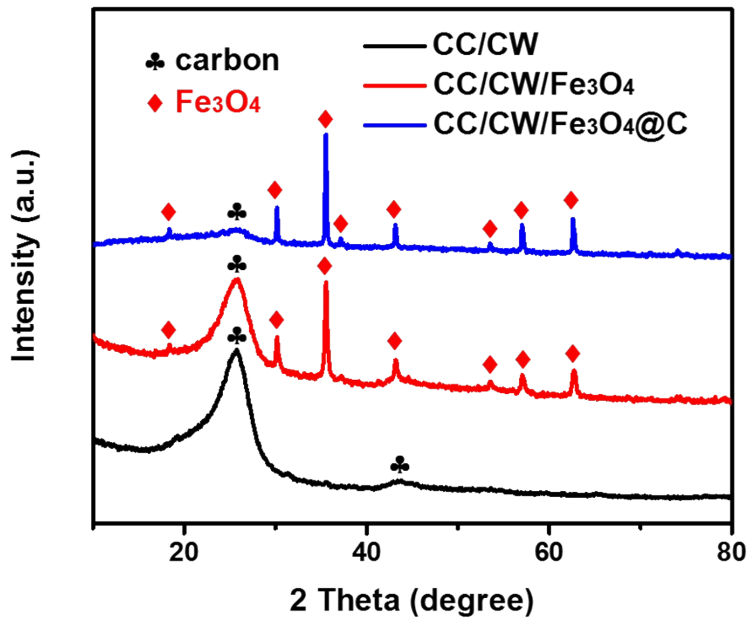

Figure S9. XRD patterns of CC/CW, CC/CW/Fe_3O_4 and CC/CW/Fe_3O_4@C.

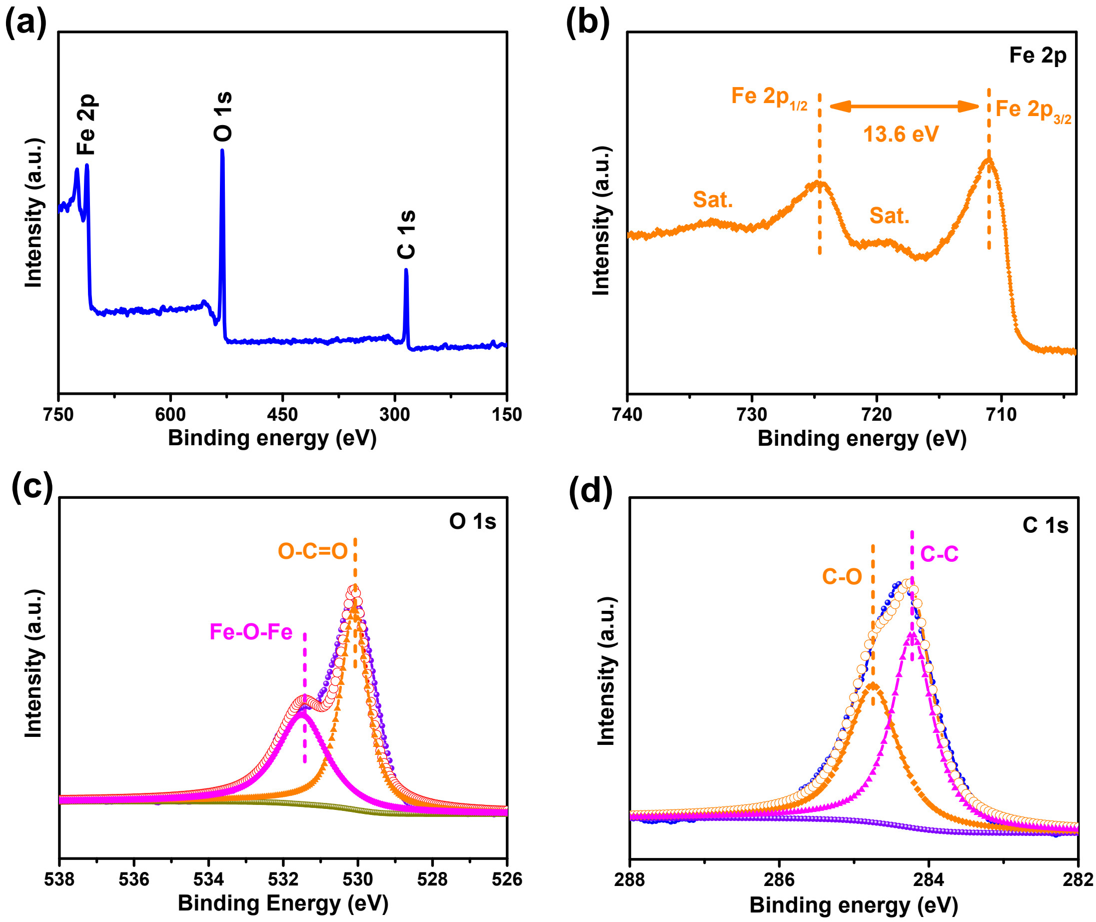

Figure S10. XPS spectra of CC/CW/Fe_3O_4@C. (a) survey, (b) Fe 2p, (c) O 1s and (d) C 1s.

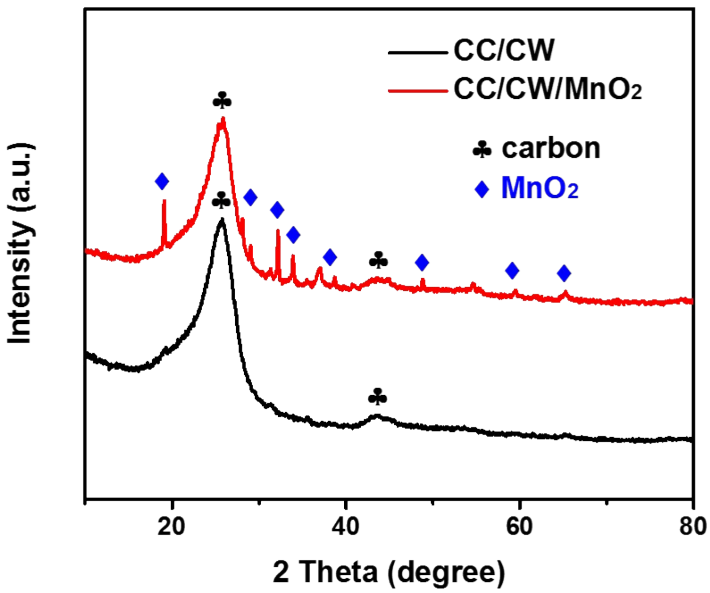

Figure S11. XRD patterns of CC/CW and CC/CW/MnO_2.

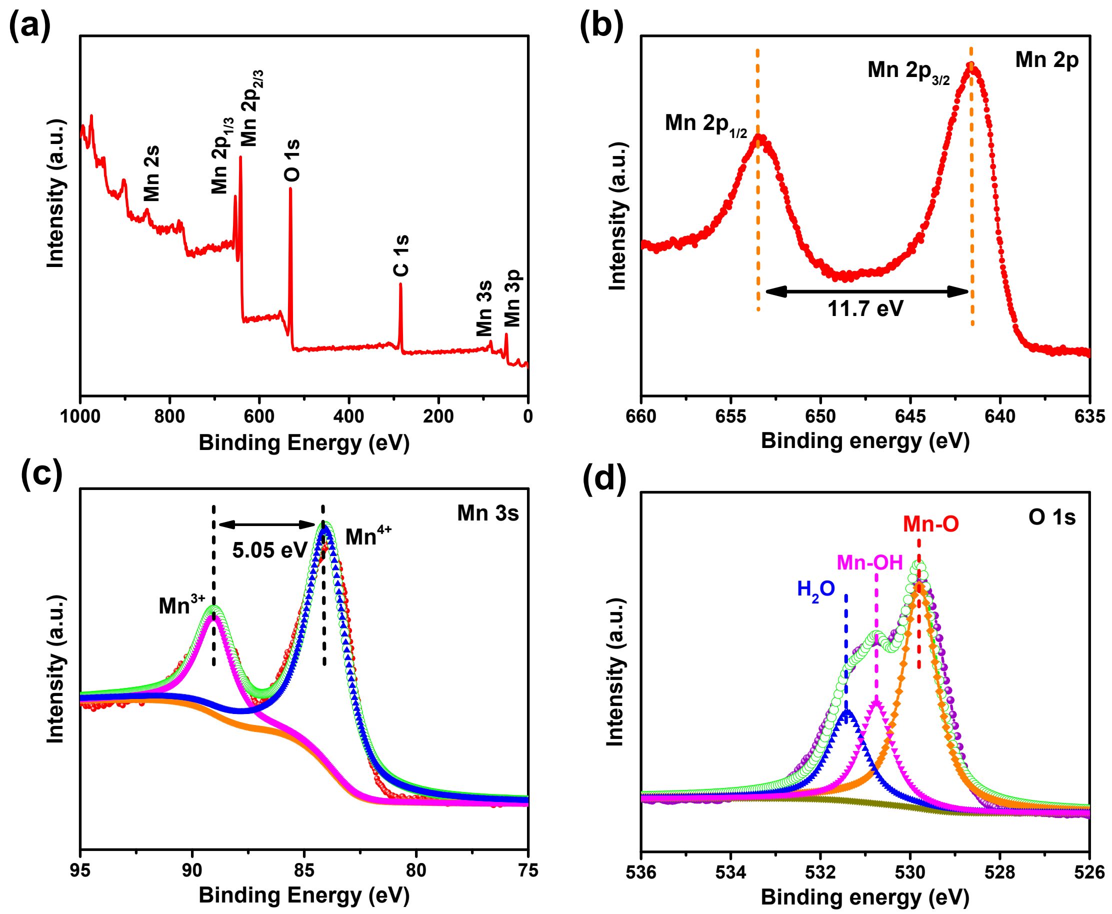

Figure S12. XPS spectra of CC/CW/MnO_2. (a) survey, (b) Mn 2p, (c) Mn 3s and (d) O 1s.

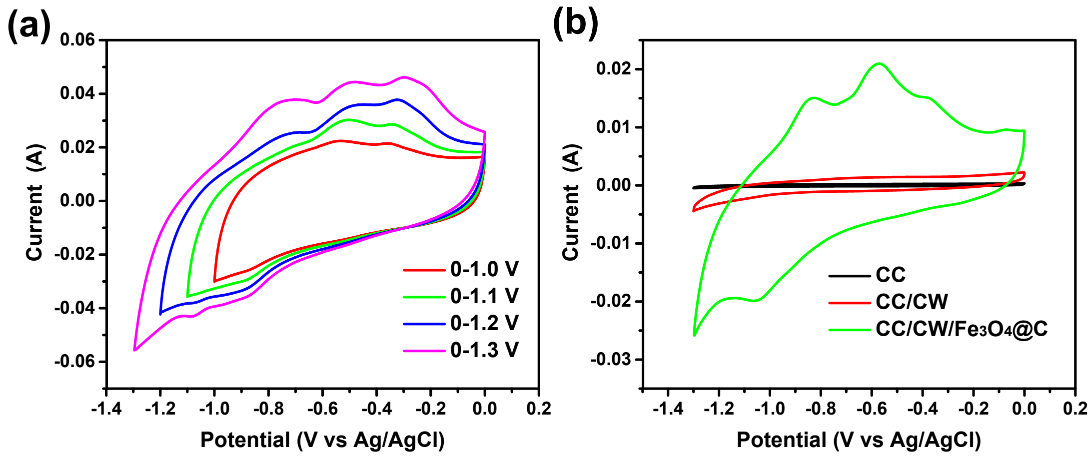

Figure S13. (a) CV curves of CC/CW/Fe_3O_4@C anode in different potential windows of -1.0 to 0, -1.1 to 0, -1.2 to 0 and -1.3 to 0 V at a same scan rate of 50 mV s^{-1}. (b) CV curves of CC, CC/CW and CC/CW/Fe_3O_4@C electrodes at a scan rate of 50 mV s^{-1}.

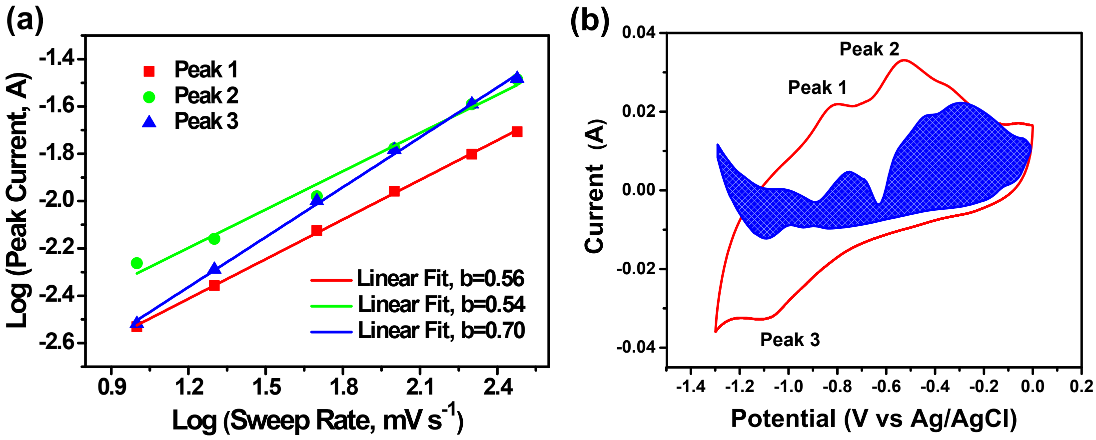

Figure S14. (a) The b-values for anodic and cathodic scans. (b) CV curve of the CC/CW/Fe_3O_4@C electrode between -1.3 and 0 V with shadowed area representing the surface capacitive contribution.

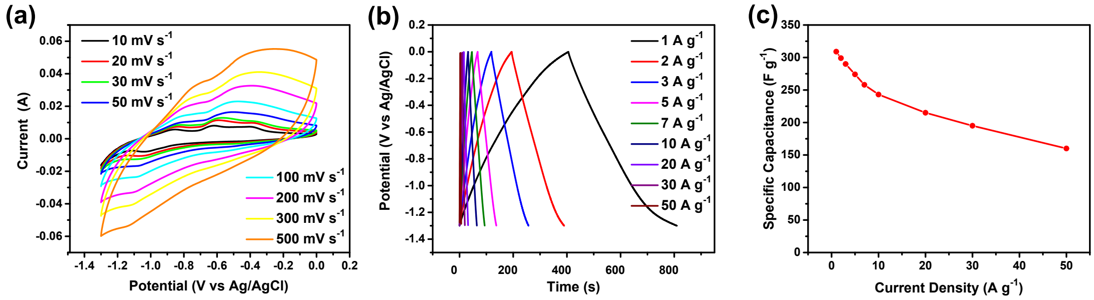

Figure S15. (a) CV curves of CC/Fe_3O_4@C electrode at different scan rates. (b) GCD curves of CC/Fe_3O_4@C electrode at different current densities. (c) Specific capacitances of CC/Fe_3O_4@C electrode calculated at different current densities.

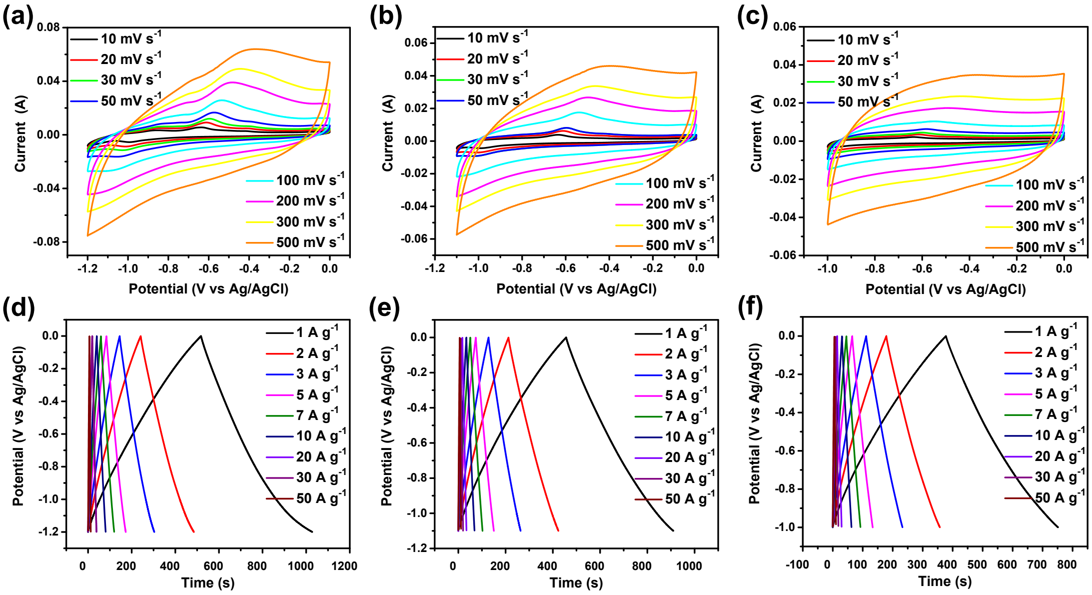

Figure S16. CV curves of the CC/CW/Fe_3O_4@C electrode in different potential windows of (a) -1.2-0 V, (b) -1.1-0 V, and (c) -1.0-0 V at different scan rates. GCD curves of the CC/CW/Fe_3O_4@C electrode in different potential windows of (d) -1.2-0 V, (e) -1.1-0 V, and (f) -1.0-0 V at different current densities.

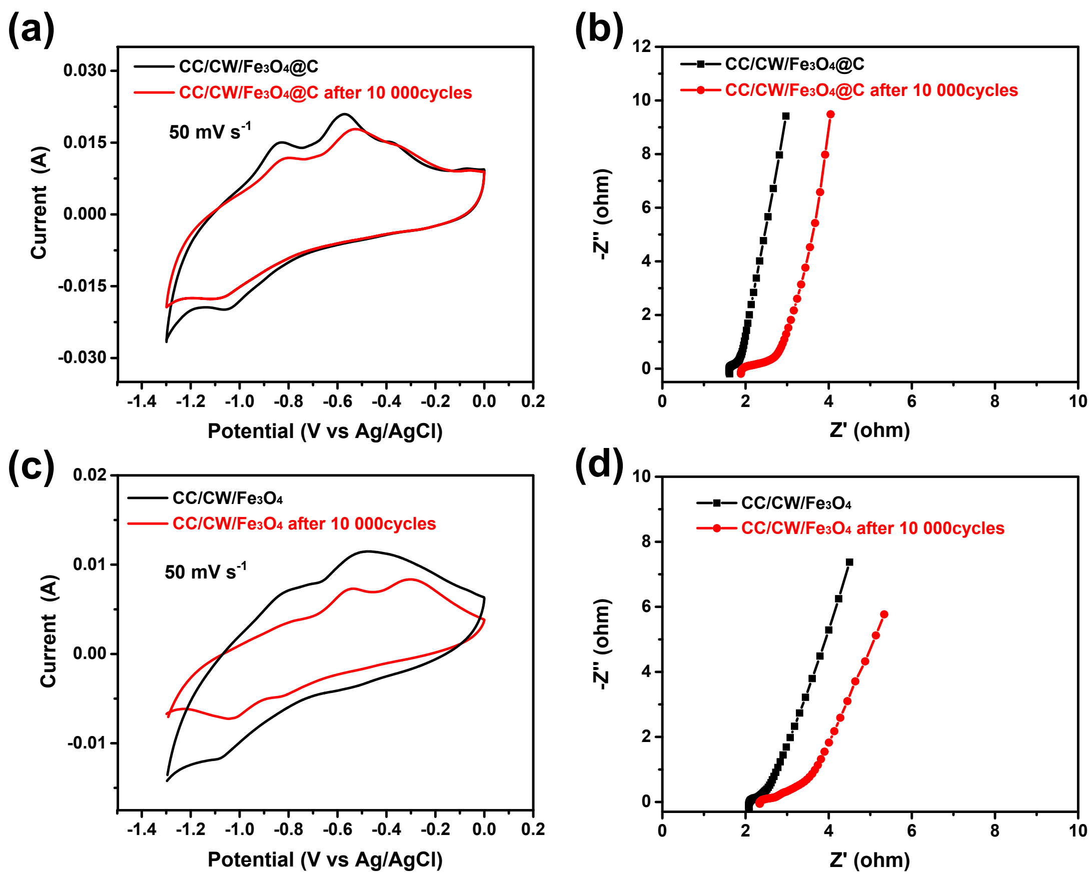

Figure S17. (a) CV and (b) EIS comparison of CC/CW/Fe_3O_4@C electrode before and after 10 000 cycles. (c) CV and (d) EIS comparison of CC/CW/Fe_3O_4 electrode before and after 10 000 cycles.

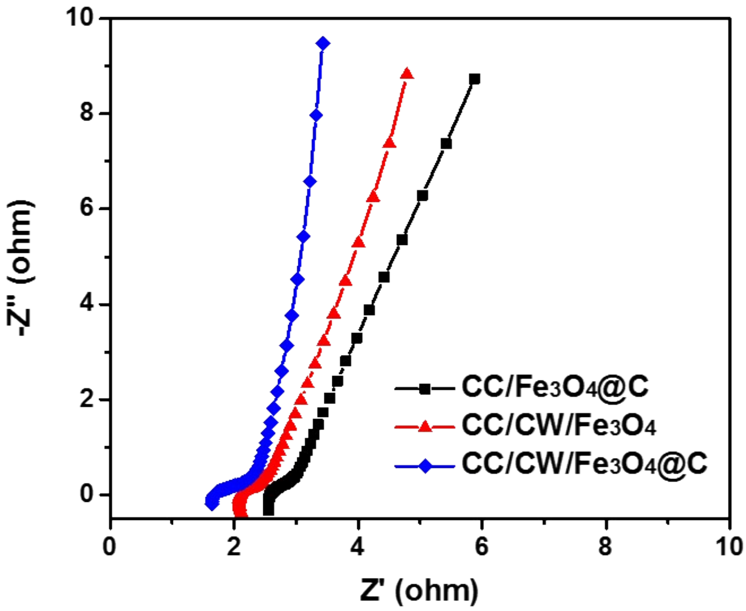

Figure S18. EIS spectra of CC/Fe_3O_4@C, CC/CW/Fe_3O_4 and CC/CW/Fe_3O_4@C electrodes.

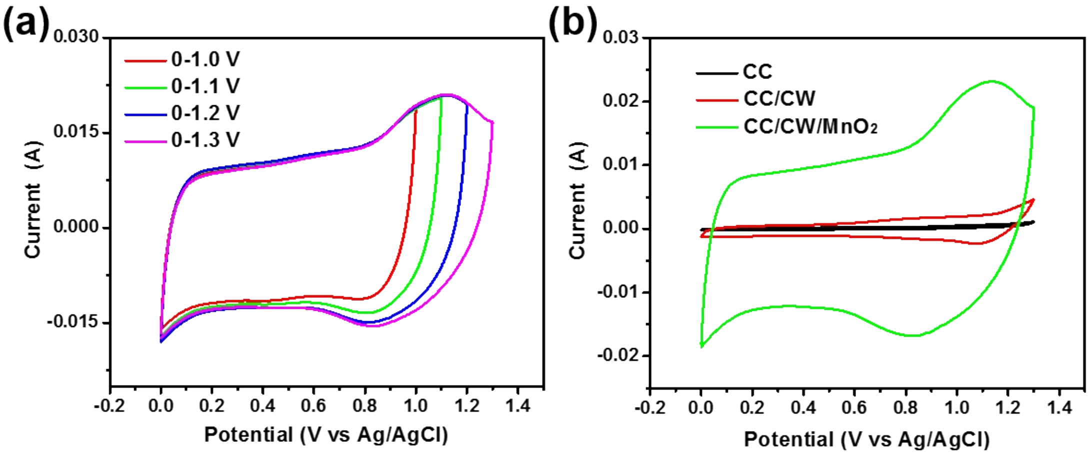

Figure S19. (a) CV curves of CC/CW/MnO_2 cathode in different potential windows at 50 mV s^{-1}. (b) CV curves of CC, CC/CW and CC/CW/MnO_2 electrodes at a scan rate of 50 mV s^{-1}.

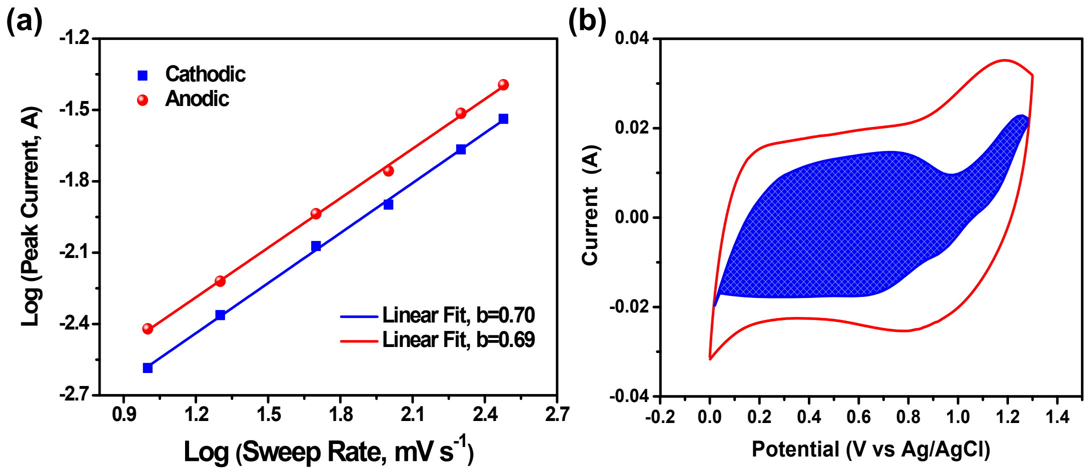

Figure S20. (a) The b-values for anodic and cathodic scans. (b) CV curve of the CC/MnO_2 electrode from 0 to 1.3 V with shadowed area representing the surface capacitive contribution.

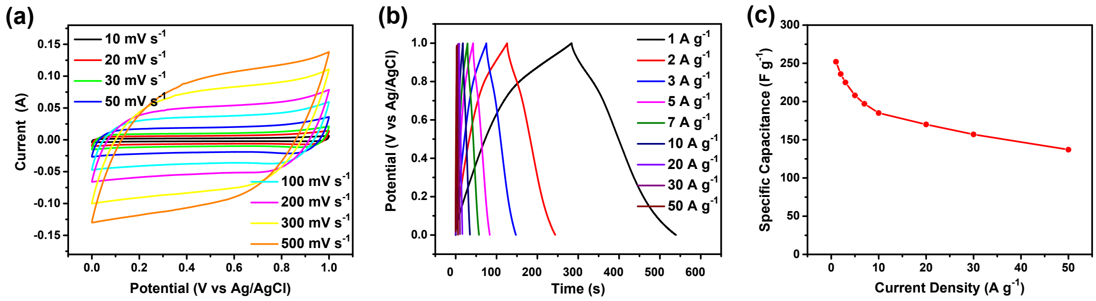

Figure S21. (a) CV curves of CC/MnO_2 electrode at different scan rates. (b) GCD curves of CC/MnO_2 electrode at different current densities. (c) Specific capacitances of CC/MnO_2 electrode calculated at different current densities.

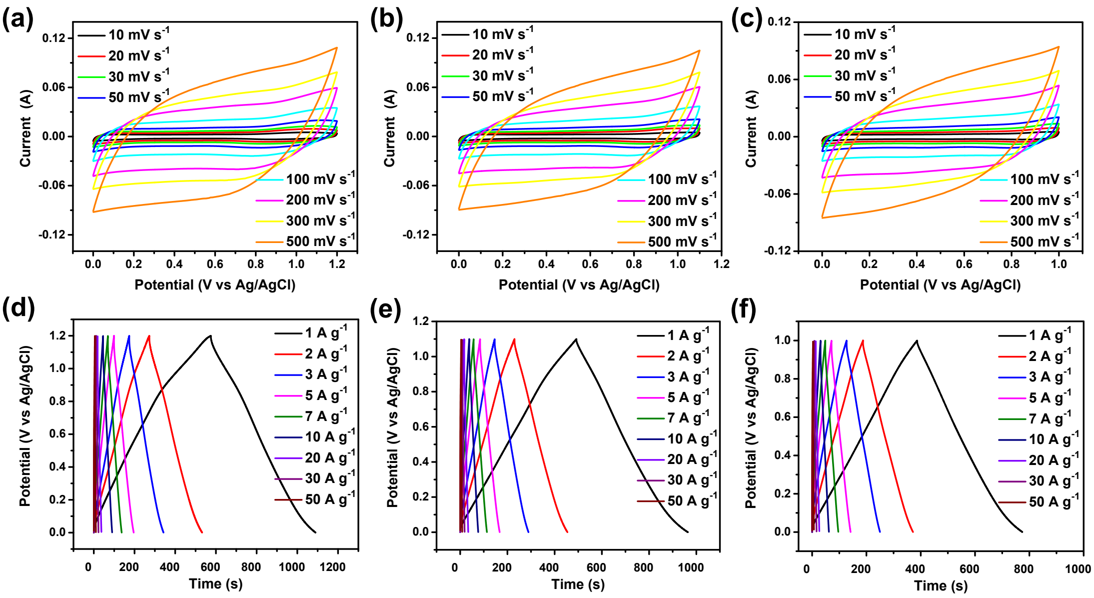

Figure S22. CV curves of the CC/CW/MnO_2 electrode in different potential windows of (a) 0-1.2 V, (b) 0-1.1 V and (c) 0-1.0 V at different scan rates. GCD curves of the CC/CW/MnO_2 electrode in different potential windows of (d) 0-1.2 V, (e) 0-1.1 V and (f) 0-1.0 V at different current densities.

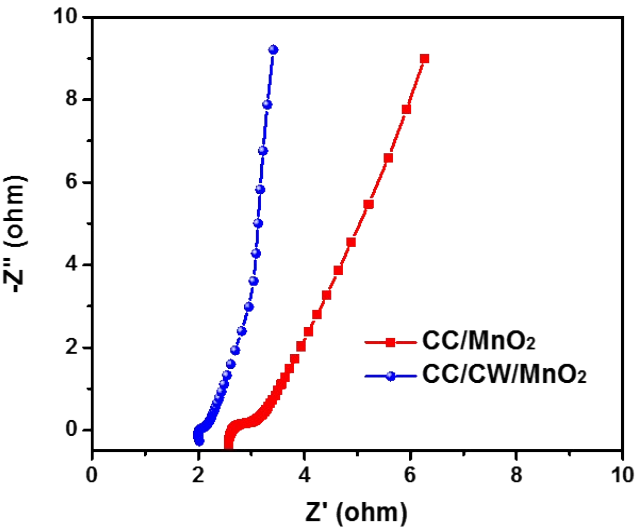

Figure S23. EIS spectra of CC/MnO_2 and CC/CW/MnO_2 electrodes.

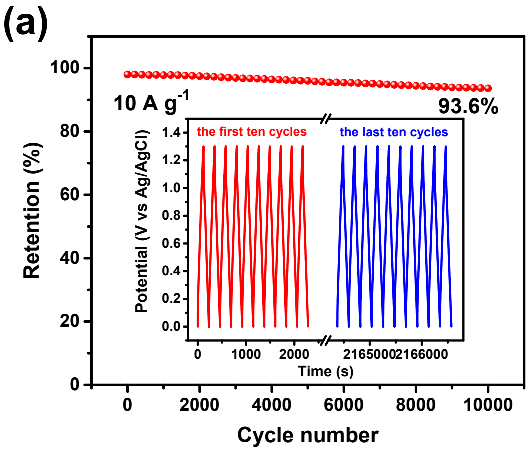

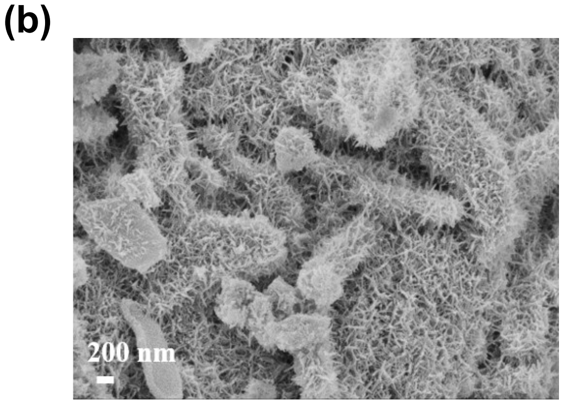

Figure S24. (a) Long term cycling stability of the CC/CW/MnO_2 electrode at a current density of 10 A g^{-1}. The inset shows GCD curves of the first ten cycles and last ten cycles. (b) SEM image of CC/CW/MnO_2 electrode after 10 000 cycling stability test.

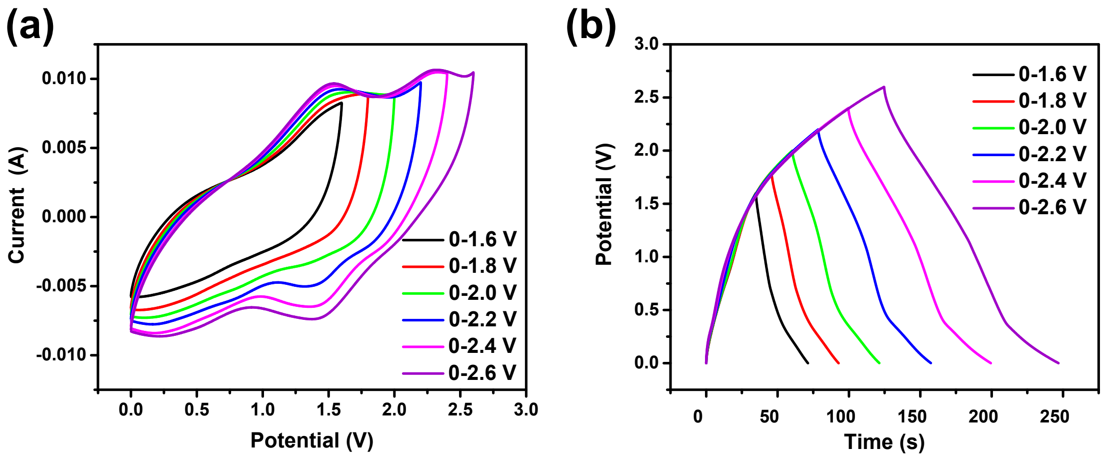

Figure S25. (a) CV curves of the CC/CW/Fe_3O_4@C//CC/CW/MnO_2 ASC in different voltage windows at a scan rate of 50 mV s^{-1}. (b) GCD curves of the CC/CW/Fe_3O_4@C//CC/CW/MnO_2 ASC in different voltage windows at a current density of 2 A g^{-1}.

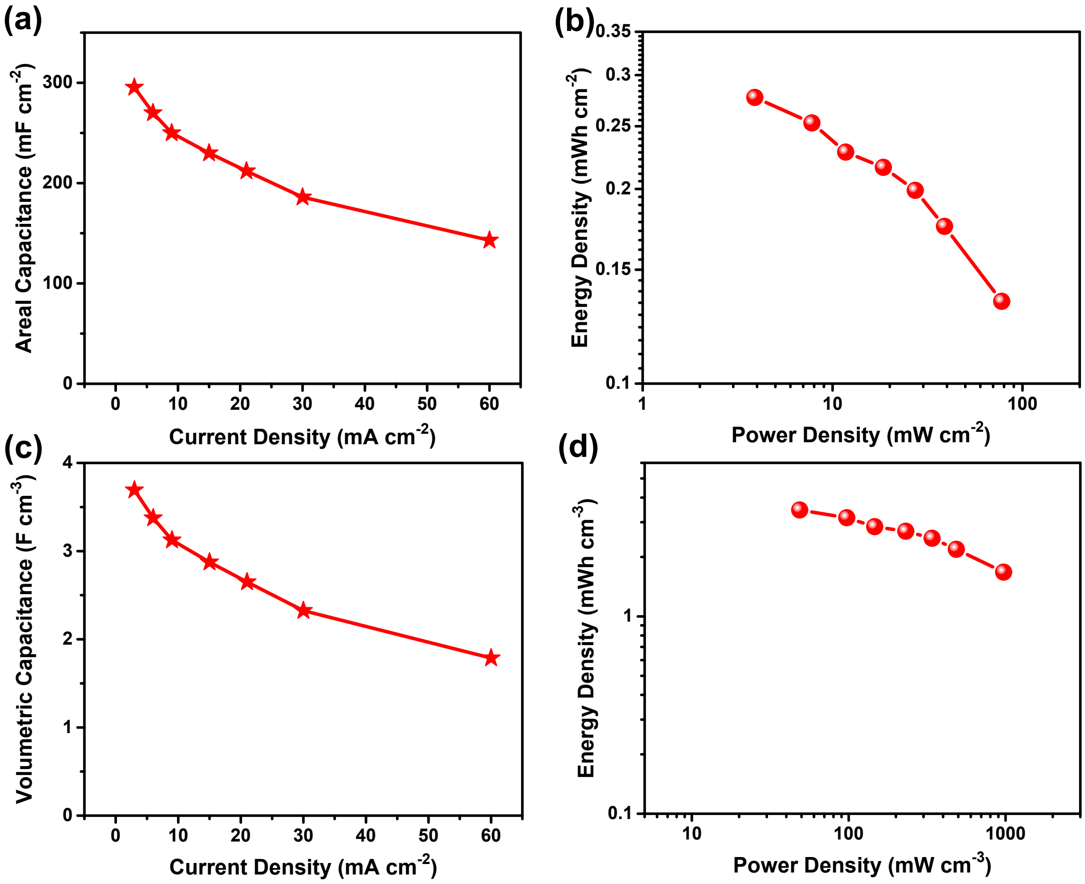

Figure S26. (a) Specific areal capacitances and (c) specific volumetric capacitances of the CC/CW/Fe_3O_4@C//CC/CW/MnO_2 ASC at different current densities. Ragon plot of the CC/CW/Fe_3O_4@C//CC/CW/MnO_2 ASC based on (b) areal energy density *vs* power density and (d) volumetric energy density *vs* power density.

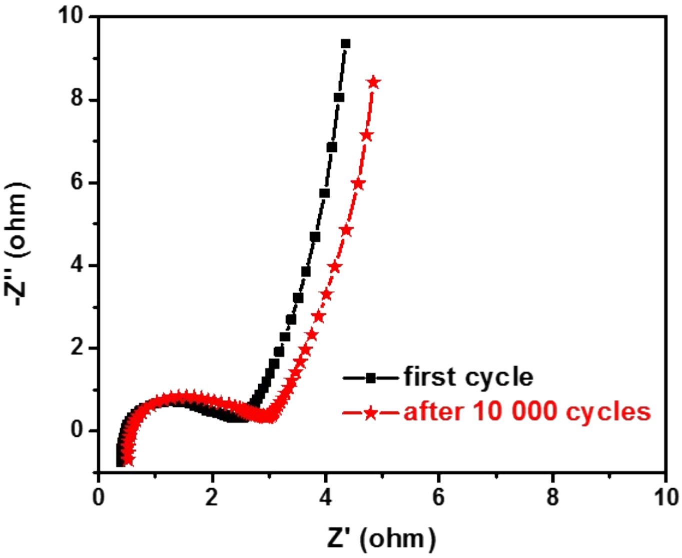

Figure S27. EIS spectra of the CC/CW/Fe_3O_4@C//CC/CW/MnO_2 ASC in initial and final cycles.

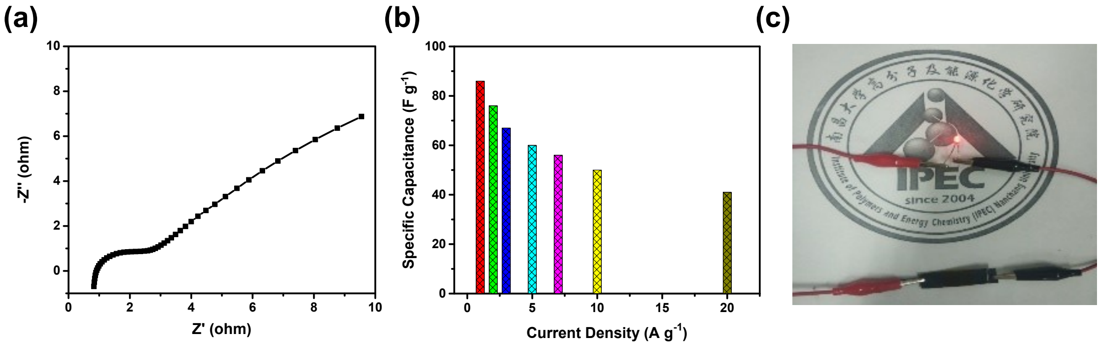

Figure S28. (a) EIS spectrum of the all-solid-state CC/CW/Fe_3O_4@C//CC/CW/MnO_2 flexible ASC. (b) Specific capacitances of the all-solid-state CC/CW/Fe_3O_4@C//CC/CW/MnO_2 flexible ASC at different current densities. (c) Photographic images of the red LED operated by a flexible ASC device.

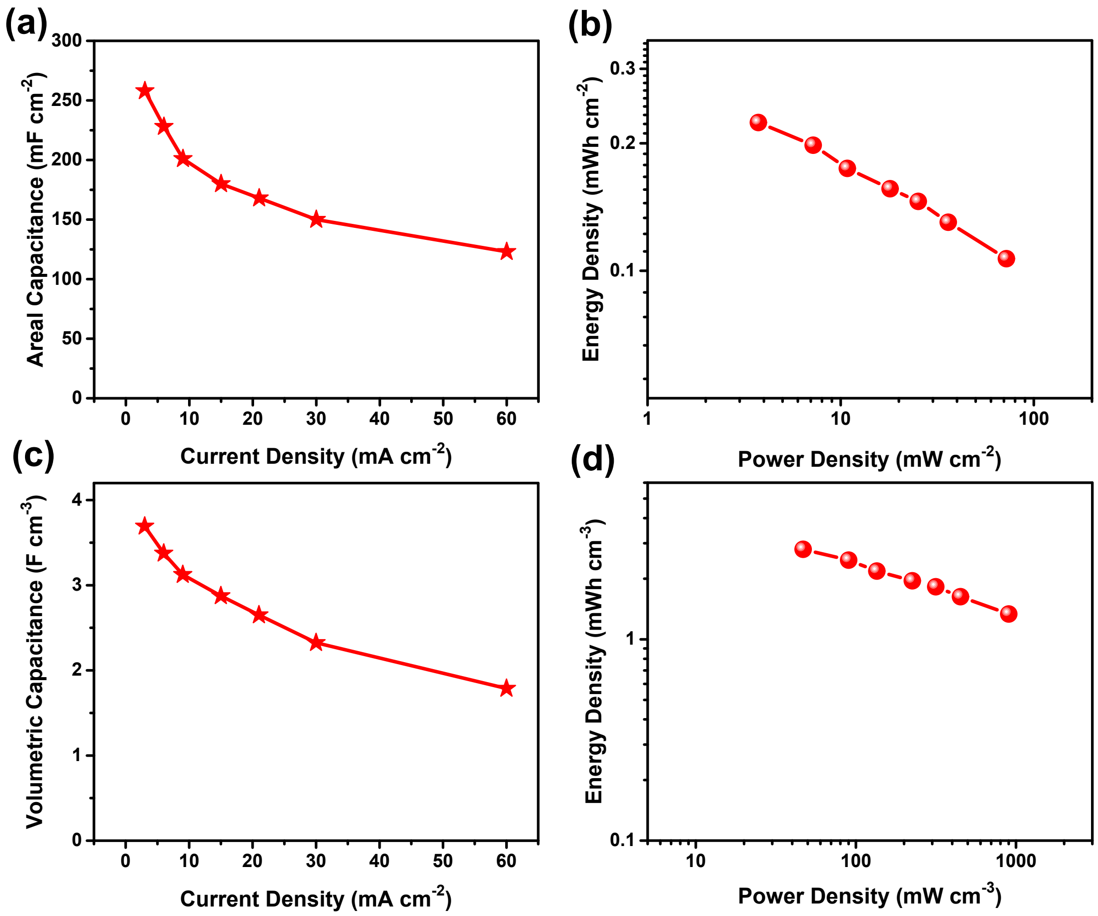

Figure S29. (a) Specific areal capacitances and (c) specific volumetric capacitances of the all-solid-state CC/CW/Fe_3O_4@C//CC/CW/MnO_2 flexible ASC at different current densities. Ragon plot of the all-solid-state CC/CW/Fe_3O_4@C//CC/CW/MnO_2 flexible ASC based on (b) areal energy density *vs* power density and (d) volumetric energy density *vs* power density.

Table S1. Electrochemical properties for CC/CW/Fe_3O_4@C in comparison with those Fe-based electrode materials in earlier reports.

Fe-based electrodes	Voltage range (V vs. Ag/AgCl or SCE)	Specific capacitance ($F\ g^{-1}$)	Rate capability ($F\ g^{-1}$)	Ref.
NiNTAs@Fe_2O_3 nanoneedles	-0.8 to 0 V	418.7 at 4 A g^{-1}	215.3 at 64 A g^{-1}	[3]
Fe_3O_4@C	-1.3 to 0 V	334 at 1 A g^{-1}	199 at 16 A g^{-1}	[4]
Porous Fe_2O_3	-1.0 to 0.2 V	375 at 10 mV s^{-1}	124 at 200 mV s^{-1}	[5]
Fe_2O_3 QDs/FGS	-1.0 to 0 V	347 at 10 mV s^{-1}	140 at 1600 mV s^{-1}	[6]
α-Fe_2O_3	-0.8 to 0 V	300 at 1 A g^{-1}	152 at 14 A g^{-1}	[7]
FeOOH/Ag/ZnO nanorods	0.8 to 0 V	376.6 at 1 A g^{-1}	126.1 at 10 A g^{-1}	[8]
γ-Fe_2O_3/graphene	-0.8 to 0 V	224 at 1 A g^{-1}	203.8 at 20 A g^{-1}	[9]
Fe_2O_3 nanoflake	-0.7 to -0 V	100.6 at 1 mA cm^{-2}	81.1 at 10 mA cm^{-2}	[10]
Fe_2O_3 nanotube	-0.8 to 0 V	257.8 at 1.4 A g^{-1}	--	[11]
α-Fe_2O_3 /graphene	-1.2 to -0.2 V	306.9 at 3 A g^{-1}	98.2 at 10 A g^{-1}	[12]
Ti-doped Fe_2O_3@PEDOT	-0.8 to 0 V	311.6 at 1 mA cm^{-2}	--	[13]
CC/CW/Fe_3O_4@C	**-1.3 to 0 V**	**463 at 1 A g^{-1}**	**296 at 50 A g^{-1}**	**This work**

Table S2. Electrochemical properties for CC/CW/MnO_2 in comparison with those Mn-based electrode materials in earlier reports.

Mn-based electrodes	**Voltage range (V vs. Ag/AgCl or SCE)**	**Specific capacitance ($F\ g^{-1}$)**	**Rate capability ($F\ g^{-1}$)**	**Ref.**
NiNTAs@MnO_2	0 to 0.8 V	400.7 at 5 mV s^{-1}	--	[3]
CC/$Na_{0.5}MnO_2$ NWAs	0 to 1.3 V	366 at 1 A g^{-1}	231 at 16 A g^{-1}	[4]
porous Mn_3O_4	-0.1 to 1.0 V	431 at 1 A g^{-1}	238 at 30 A g^{-1}	[5]
MnO_2/GO	-0.1 to 0.9 V	297 at 5 mV s^{-1}	268 at 50 mV s^{-1}	[14]
MnO_2@PPy NWs	0 to 0.9 V	325 at 1 A g^{-1}	200 at 20 A g^{-1}	[15]
rGO@Mn_3O_4	-0.1 to 1.2 V	288 at 0.7 A g^{-1}	174 at 24 A g^{-1}	[16]
GrMnO_2	-0.1 to 0.9 V	350 at 0.2 A g^{-1}	162 at 10 A g^{-1}	[17]
HCC@MnO_2	0 to 0.8 V	243 at 1 A g^{-1}	139 at 10 A g^{-1}	[18]
Porous Mn_3O_4	-0.1 to 0.55 V	376.6 at 0.1 A g^{-1}	166 at 50 A g^{-1}	[19]
3D MnO_2/Graphene	0 to 0.8 V	422.5 at 1 A g^{-1}	228.8 at 10 A g^{-1}	[20]
MnO_x@C@MnO_x	-0.1 to 0.55 V	350 at 1 A g^{-1}	122 at 20 A g^{-1}	[21]
α-MnO_2	0 to 0.9 V	304 at 3 mA cm^{-2}	--	[22]
CC/CW/MnO_2	**0 to 1.3 V**	**481 at 1 A g^{-1}**	**270 at 50 A g^{-1}**	**This work**

Table S3. Comparison study on the electrochemical performance of asymmetric aqueous supercapacitor in this work with previously reported results.

Active materials	**Electrolyte**	**Potential (V)**	***E* (Wh kg^{-1})**	***P* (W kg^{-1})**	**Capacitance retention (after cycles)**	**Ref.**
Ni@Fe_2O_3//Ni@MnO_2	1 M Na_2SO_4	0~1.6	34.1	3197.7	92.3% (5000)	[3]
$Na_{0.5}MnO_2$//Fe_3O_4@C	1 M Na_2SO_4	0~2.6	81	647	93% (10000)	[4]
porous Mn_3O_4 porous Fe_2O_3	1 M Na_2SO_4	0~2.0	74.2	998	--	[5]
MnO_2/GO//HPC	1 M Na_2SO_4	0~2.0	46.7	100	93% (4000)	[14]
PPy/MnO_2//AC	1 M Na_2SO_4	0~1.8	25.8	9000	90.3% (6000)	[15]
rGO@Mn_3O_4//rGO@VO_2	1 M Na_2SO_4	0~2.2	42.7	11260	--	[16]
Graphene/MnO_2//Graphene/MoO_3	1 M Na_2SO_4	0~2.0	42.6	276	--	[17]
HCC@MnO_2//HCC@PPy	PVA/LiCl	0~1.8	28.2	420.5	91.2% (5000)	[18]
Mn_3O_4//NC	6 M KOH	0~1.5	17.2	4255	--	[19]
MnO_2/ERGO//CNT/ERGO	PAAK/KCl	0~1.8	31.8	453.6	88.4% (10000)	[20]
MnO_2@CNT//MoO_3@CNT	1 M Na_2SO_4	0~2.0	27.8	10000	96.8% (10000)	[23]
Graphene/MnO_2//graphene	1 M Na_2SO_4	0~2.0	30	5000	79% (1000)	[24]
Bi_2O_3/CNF//MnO_2/CNF	1 M Na_2SO_4	0~1.8	11.3	3370	85% (4000)	[25]
β-MnO_2//AGO	1 M Na_2SO_4	0~2.2	40.4	275	85.7% (5000)	[26]
3D MnO_2//AC	PVA/ Na_2SO_4	0~1.7	40.2	6227	90% (8000)	[27]
Fe_2O_3/FGS//MnO_2/FGS	1 M Na_2SO_4	0~2.0	50.7	100	95% (5000)	[28]
CNT/MnO_2//CNT/polypyrrole	0.5 M Na_2SO_4	0~1.6	22.8	860	90.2% (10000)	[29]
MnO_2//nitrogen-doped carbon	1 M Na_2SO_4	0~2.0	32.9	284.6	95.4% (2000)	[30]
RGO-RuO_2//RGO-polyaniline	2 M H_2SO_4	0~1.4	26.3	150	--	[31]
MnO_2/CNT//In_2O_3/CNT	1 M Na_2SO_4	0~2.2	22.5	--	--	[32]
CW/MnO_2//CW/Fe_3O_4@C	**1 M Na_2SO_4**	**0~2.6**	**91.1**	**3197**	**92.8%** (10000)	**This work**

Table S4. Comparison study on the electrochemical performance of asymmetric aqueous supercapacitor in this work with previously reported results.

Active materials	Electrolyte	Potential (V)	*E* (mWh cm^{-3})	*P* (W cm^{-3})	Ref.
MnO_2//Ti-Fe_2O_3@PEDOT	LiCl/PVA	0~1.6	0.89	0.44	[13]
PANI//WO_{3-x}/MoO_{3-x}	H_3PO_4/PVA	0~1.9	1.10	0.73	[33]
MVNN/CNT//MVNN/CNT	H_3PO_4/PVA	0~0.7	0.54	0.40	[34]
VO_x//VN	LiCl/PVA	0~2.2	0.61	0.85	[35]
MnO_2@TiN//PVO	LiCl/PVA	0~1.8	1.93	2.71	[36]
H-TiO_2@MnO_2//H-TiO_2@C	H_3PO_4/PVA	0~1.8	0.3	0.23	[37]
ASV-FO//V-CO	LiOH/PVA	0~1.6	0.95	0.02	[38]
MnO_2@TiN//EACC	5 M LiCl	0~2.0	1.50	1.71	[39]
VO_x@MoO_3/FEG//MnO_2/CEG	5 M LiCl	0~2.3	3.02	0.033	[40]
CW/MnO_2//CW/Fe_3O_4@C	**1 M Na_2SO_4**	**0~2.6**	**3.40**	**0.049**	**This work**
CW/MnO_2//CW/Fe_3O_4@C	**Na_2SO_4/CMC**	**0~2.5**	**2.8**	**0.047**	**This work**

References

1. T. Brezesinski, J. Wang, S. H. Tolbert and B. Dunn, *Nat. Mater.*, 2010, **9**, 146.
2. V. Augustyn, P. Simon and B. Dunn, *Energy Environ. Sci.*, 2014, **7**, 1597-1614.
3. Y. Li, J. Xu, T. Feng, Q. Yao, J. Xie and H. Xia, *Adv. Funct. Mater.*, 2017, **27**, 1606728.
4. N. Jabeen, A. Hussain, Q. Xia, S. Sun, J. Zhu and H. Xia, *Adv. Mater.*, 2017, **29**, 1700804.
5. J. W. Choi, I. W. Ock, K. H. Kim, H. M. Jeong and J. K. Kang, *Adv. Funct. Mater.*, 2018, **28**, 1803695.
6. H. Xia, C. Hong, B. Li, B. Zhao, Z. Lin, M. Zheng, S. V. Savilov and S. M. Aldoshin, *Adv. Funct. Mater.*, 2015, **25**, 627-635.
7. S. Shivakumara, T. R. Penki and N. Munichandraiah, *Mater. Lett.*, 2014, **131**, 100-103.
8. S. Yang, Y. Li, T. Xu, Y. Li, H. Fu, K. Cheng, K. Ye, L. Yang, D. Cao and G. Wang, *RSC Adv.*, 2016, **6**, 39166-39171.
9. H. C. Chen, C. C. Wang and S. Y. Lu, *J. Mater. Chem. A*, 2014, **2**, 16955-16962.
10. T. Liu, Y. Ling, Y. Yang, L. Finn, E. Collazo, T. Zhai, Y. Tong and Y. Li, *Nano Energy*, 2015, **12**, 169-177.
11. P. Yang, Y. Ding, Z. Lin, Z. Chen, Y. Li, P. Qiang, M. Ebrahimi, W. Mai, C. P. Wong and Z. L. Wang, *Nano Lett.*, 2014, **14**, 731-736.
12. S. Yang, X. Song, P. Zhang, J. Sun and L. Gao, *Small*, 2014, **10**, 2270-2279.
13. Y. Zeng, Y. Han, Y. Zhao, Y. Zeng, M. Yu, Y. Liu, H. Tang, Y. Tong and X. Lu, *Adv. Energy Mater.*, 2015, 1402176.
14. Y. Zhao, W. Ran, J. He, Y. Huang, Z. Liu, W. Liu, Y. Tang, L. Zhang, D. Gao and F. Gao, *Small*, 2015, **11**, 1310-1319.
15. W. He, C. Wang, F. Zhuge, X. Deng, X. Xu and T. Zhai, *Nano Energy,* 2017, **35**, 242-250.
16. R. Sahoo, D. T. Pham, T. H. Lee, T. H. T. Luu, J. Seok and Y. H. Lee, *ACS Nano*, 2018, **12**, 8494-8505.
17. J. Chang, M. Jin, F. Yao, T. H. Kim, V. T. Le, H. Yue, F. Gunes, B. Li, A. Ghosh,

S. Xie and Y. H. Lee, *Adv. Funct. Mater.*, 2013, **23**, 5074-5083.
18. Z. Chen, L. Zheng, T. Zhu, Z. Ma, Y. Yang, C. Wei, L. Liu and X. Gong, *Adv. Electron. Mater.*, 2019, **5**, 1800721.
19. G. Wang, Z. Ma, Y. Fan, G. Shao, L. Kong and W. Gao, *Phys. Chem. Chem. Phys.*, 2015, **17**, 23017-23025.
20. Z. Zhang, F. Xiao, L. Qian, J. Xiao, S. Wang and Y. Liu, *Adv. Energy Mater.*, 2014, **4**, 1400064.
21. Z. Ma, F. Jing, Y. Fan, L. Hou, L. Su, L. Fan and G. Shao, *Small*, 2019, **15**, 1900862.
22. Z. H. Huang, Y. Song, D. Y. Feng, Z. Sun, X. Sun and X. X. Liu, *ACS Nano*, 2018, **12**, 3557-3567.
23. T. H. Lee, D. T. Phama, R. Sahoo, J. Seok, T. H. T. Luu and Y. H. Lee, *Energy Storage Mater.*, 2018, **12**, 223-231.
24. Z. S. Wu, W. Ren, D. W. Wang, F. Li, B. Liu and H. M. Cheng, *ACS Nano*, 2010, **4**, 5835-5842.
25. H. Xu, X. Hu, H. Yang, Y. Sun, C. Hu, and Y. Huang, *Adv. Energy Mater.*, 2015, **5**, 1401882.
26. S. Zhu, L. Li, J. Liu, H. Wang, T. Wang, Y. Zhang, L. Zhang, R. S. Ruoff and F. Dong, *ACS Nano*, 2018, **12**, 1033-1042.
27. N. Liu, Y. Su, Z. Wang, Z. Wang, J. Xia, Y. Chen, Z. Zhao, Q. Li and F. Geng, *ACS Nano*, 2017, **11**, 7879-7888.
28. H. Xia, C. Hong, B. Li, B. Zhao, Z. Lin, M. Zheng, S. V. Savilov and S. M. Aldoshin, *Adv. Funct. Mater.*, 2015, **25**, 627-635.
29. J. Liu, L. Zhang, H. B. Wu, J. Lin, Z. Shen and X. W. Lou, *Energy Environ. Sci.*, 2014, **7**, 3709-3719.
30. L. F. Chen, Z. H. Huang, H. W. Liang, Q. F. Guan and S. H. Yu, *Adv. Mater.*, 2013, **25**, 4746-4752.
31. J. Zhang, J. Jiang, H. Li and X. S. Zhao, *Energy Environ. Sci.*, 2011, **4**, 4009-4015.
32. P. C. Chen, G. Shen, Y. Shi, H. Chen and C. Zhou, *ACS Nano*, 2010, **4**, 4403-4411.

33. X. Xiao, T. Ding, L. Yuan, Y. Shen, Q. Zhong, X. Zhang, Y. Cao, B. Hu, T. Zhai, L. Gong, J. Chen, Y. Tong, J. Zhou, and Z. L. Wang, *Adv. Energy Mater*., 2012, **11**, 1328-1332.
34. X. Xiao, X. Peng, H. Jin, T. Li, C. Zhang, B. Gao, B. Hu, K. Huo, and J. Zhou, *Adv. Mater*., 2013, **25**, 5091-5097.
35. X. Lu, M. Yu, T. Zhai, G. Wang, S. Xie, T. Liu, C. Liang, Y. Tong, and Y. Li, *Nano Lett*., 2013, **13**, 2628-2633.
36. K. Zheng, Y. Zeng, S. Liu, C. Zeng, Y. Tong, Z. Zheng, T. Zhu and X. Lu, *Energy Storage Mater*., 2019, **22**, 410-417.
37. X. Lu, M. Yu, G. Wang, T. Zhai, S. Xie, Y. Ling, Y. Tong, and Y. Li, *Adv. Mater*., 2013, **25**, 267-272.
38. S. Sun, T. Zhai, C. Liang, S. V. Savilov, H. Xia, *Nano Energy*, 2018, **45**, 390-397.
39. W. Wang, W. Liu, Y. Zeng, Y. Han, M. Yu, X. Lu, and Y. Tong, *Adv. Mater*., 2015, **27**, 3572-3578.
40. S. Q. Wang, X. Cai, Y. Song, X. Sun, and X. X. Liu, *Adv. Funct. Mater*., 2018, **28**, 1803901-1803907.